ZEUS Results

Elisabetta Gallo[†]

INFN Firenze, Italy
(On behalf of the ZEUS Collaboration)

Abstract. Several results from the ZEUS Collaboration were presented at this Workshop. The highlights are presented in this summary, and include results from NLO QCD fits and determination of α_S, from forward jets and diffractive final states, from pentaquarks and searches and from heavy flavour production. Also the first results from the analysis of the HERA II e^+p/e^-p data are shown.

Keywords: Document processing, Class file writing, LaTeX 2_ε
PACS: 43.35.Ei, 78.60.Mq

INTRODUCTION

These proceedings report on the highlights of recent results from the ZEUS Collaboration. The published structure functions data have been used to determine the proton parton distribution functions in NLO QCD fits. The fit includes also jet data to constrain the gluon in the middle-x region. The strong coupling constant α_S is determined in various measurements. The diffractive parton distribution functions are also determined from inclusive data and used to obtain predictions for diffractive final states. ZEUS has performed searches for exotic final states like pentaquarks, involving strange or charm quarks. The HERA experiments are still competitive in the search for SUSY with R-parity-violating interactions and the recent search for stop is described. Several results on heavy flavour production were presented in the parallel sections, here the results on beauty cross sections at HERA I and D^* production at HERA II are reported. Finally the first results on the charged current polarized cross sections are shown.

STRUCTURE FUNCTIONS AND JETS

NLO QCD fits

The ZEUS Collaboration has completed the publication of the structure function data from the HERA I (94-00) running. These cross sections have been used in a NLO QCD fit, based on the DGLAP evolution, to determine the proton parton distributions functions (PDFs), using the ZEUS data only [1]. Uncertainties from heavy-target corrections, present in global analyses which include also fixed-target data, are therefore avoided. While the low Q^2 neutral current (NC) data determine the low-x sea and gluon distributions, the high Q^2 NC and charged (CC) cross sections constrain the valence distributions. In addition, published jet cross sections from the 96-97 data were used to constrain the gluon density in the mid-to-high-x region ($x \simeq 0.01 - 0.5$). The predictions for the

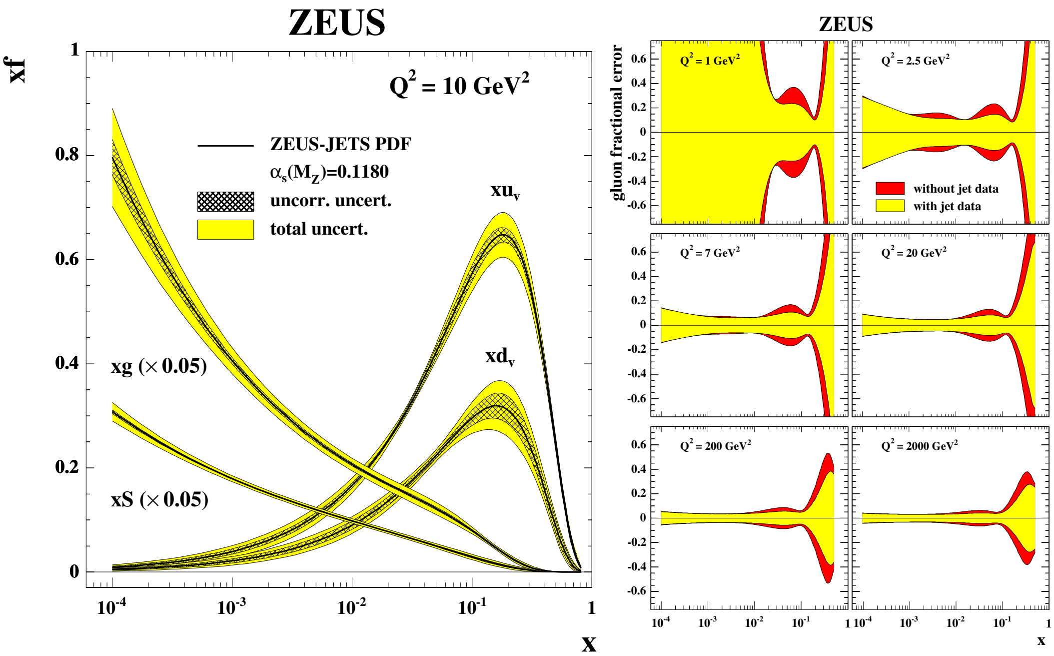

FIGURE 1. On the left: parton distribution functions for the u-valence, d-valence, sea and gluon density obtained from the ZEUS-JETS fit, for a Q^2 value of 10 GeV^2. On the right side: uncertainty on the gluon density for different values of Q^2 and for the two cases in which the jets are included or not in the fit.

two jet cross sections used (DIS jets in the Breit frame and jets in direct photoproduction) were calculated to NLO and used in the fit in a rigourous way. The resulting PDFs in this fit (see figure 1), called ZEUS-JETS fit, give a very good description of both inclusive and jet cross sections, in agreement with QCD factorization. The gain in using the jets is shown in the right part of figure 1, where the yellow (light) band shows the total experiment uncertainty on the gluon density in the fit including the jets, compared to the red (dark) band which is the error for the fit without including the jets. As an example, in the bin at $Q^2 = 7$ GeV^2 and $x \simeq 0.06$, the uncertainty is reduced from 17% to 10% using the jets. A similar decrease of approximately a factor two is visible in the whole Q^2 range in the mid-to-high-x region.

In the inclusive cross sections, there is a strong correlation between α_S and the gluon density. As the jets data depend on α_S and on $xg(x)$ in a different way, the addition of the jets data to the fits permits also a more precise determination of the strong coupling constant, compared to previous fits, when α_S is left as a free parameter. The value resulting from this fit, called ZEUS-JETS-α_S, is

$$\alpha_S(M_Z) = 0.1183 \pm 0.0028(\text{exp.}) \pm 0.0008(\text{model}) \pm 0.005(\text{scale}) \qquad (1)$$

which is in very good agreement with the world average of 0.1182 ± 0.0027.

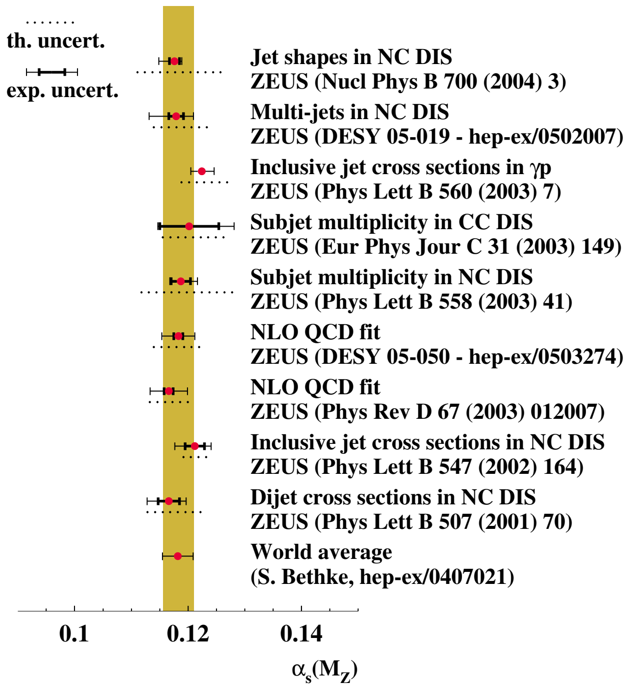

FIGURE 2. Compilation of ZEUS results on the determination of α_S. The band shows the world average as calculated in the reference cited in the figure.

Summary of α_S results

Figure 2 shows a compilation of results on the determination of α_S at ZEUS (see also [2]). The most precise result, from the experimental point of view, comes from the inclusive jets in photoproduction. Although each of the measurements has a precise experimental determination (typically 3%), competitive with the world average, the error is dominated by the theoretical uncertainties (typically 4%), which are shown by the dashed lines. NNLO (next-to-NLO) calculations for jet based variables and for PDFs are therefore needed.

Forward jets at low-x

The DGLAP evolution scheme describes the HERA structure function data down to low-x. In order to disentangle the effect of different evolution schemes, like BFKL or CCFM, it has been suggested long ago by Mueller [3] to look at jets in the forward (proton) region, where the differences between the different parton evolution schemes should be more prominent. For such an analysis, the jets were reconstructed with the k_T cluster algorithm in the longitudinally invariant inclusive mode in the Breit frame and then boosted to the laboratory frame. Thanks to the forward plug calorimeter installed for

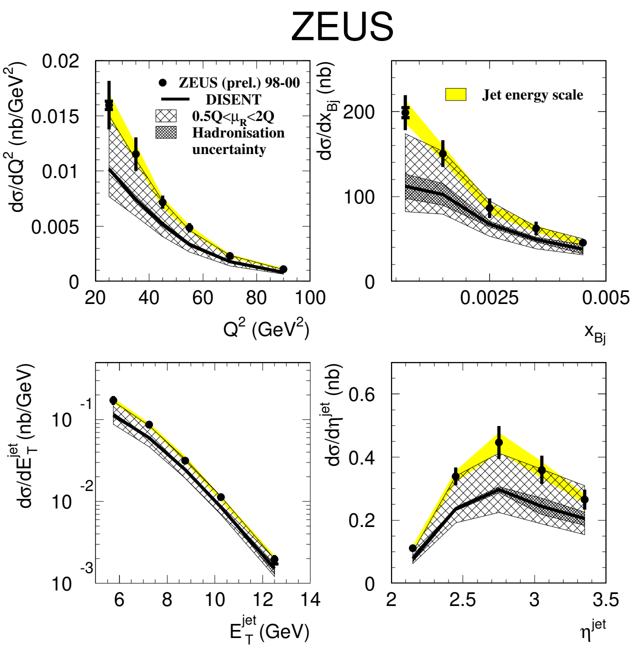

FIGURE 3. Measured differential cross sections compared to the NLO QCD calculations for forward jet production at low x.

the period 98-00, jets could be selected with a pseudorapity coverage in the laboratory frame of $2 < \eta_{\rm jet} < 3.5$. In order to enhance the contribution of possible BFKL effects, the jets were required to have a $x_{\rm jet} > x$, where $x_{\rm jet}$ is the ratio of the longitudinal momentum of the jet and the proton momentum, and x is the Bjorken variable. This requirement maximises the phase space for BFKL evolution. In addition the jets were required to have a transverse momentum squared $(E_T^{\rm jet})^2$ approximately equal to Q^2 in order to suppress DGLAP evolution as this cut leaves no room for evolution in Q^2. The events were selected in the kinematic region $20 < Q^2 < 100$ GeV^2 and $0.0004 < x < 0.005$. The differential cross sections as a function of Q^2, x, $E_T^{\rm jet}$ and $\eta_{\rm jet}$ are shown in figure 3, compared to NLO QCD calculations based on the DGLAP evolution, with the program DISENT. The data are slightly above the theoretical NLO calculations, especially in the lowest x bin, however the uncertainties on the theory are still very large, as shown by the hatched bands. The variation of the calculations due to the change of renormalization scale is particularly large, which indicates the need for higher-oder calculations.

Very high-x at HERA

While HERA has provided precision results on structure functions at low-x, the high-x region has still to be explored, because of both limited statistics and difficulty in reconstructing the kinematic variables. ZEUS has developed a new method to select

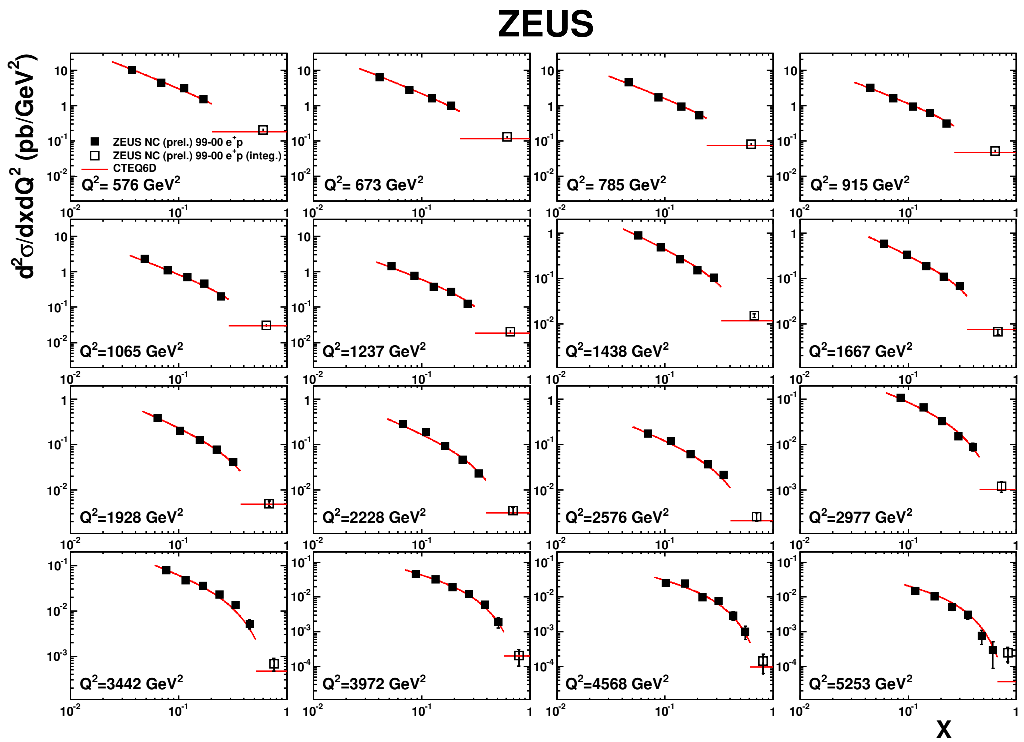

FIGURE 4. Double differential cross sections (solid squares) for the 99-00 e^+p data, as a function of x in Q^2 bins, compared to the CTEQ6D parton distributions. The last bin (open symbol) shows the integrated cross section over x divided by the bin width, i.e. $1/(1-x_{edge}) \cdot \int_{x_{edge}}^{1} (d^2\sigma/dxdQ^2)dx$; the symbol is shown at the centre of the bin. In this bin the prediction is drawn as an horizontal line. The error bars represent the quadratic sum of the statistical and systematic uncertainties.

events at very high-x and in the middle Q^2 region ($Q^2 > 576$ GeV^2). These events are characterized by a well measured scattered electron or positron in the central part of the calorimeter; and by a jet, very forward, close to the proton beampipe. As x increases, the jet is more and more boosted in the forward direction and eventually disappears in the beam pipe; the value of x at which this occurs is Q^2 dependent. The kinematic of the event is reconstructed in this way. First the Q^2 of the event is determined from the electron variables E_e and θ_e, which are measured with good resolution. The events are then separated in those with exactly one good reconstructed jet and those without any jet. For the 1-jet events, the jet information is used to calculate the Bjorken x variable from E_{jet} and θ_{jet} and the double differential cross section $d^2\sigma/dxdQ^2$ is calculated in each x, Q^2 bin. For the 0-jet sample, it is assumed that the events come from very high-x, with a lower value x_{edge} which can be evaluated for each Q^2 bin based on kinematic constraints. In this case the events are collected in a bin $x_{\text{edge}} < x < 1$ and an integrated cross section $\int_{x_{\text{edge}}}^{1} (d^2\sigma/dxdQ^2)dx$ is calculated.

The result is shown in figure 4, where, for each Q^2, the open squares in the last bin are the integrated cross sections up to $x = 1$ and the closed squares show the double differential cross section in x, Q^2. The precision in the last bin is comparable to the other

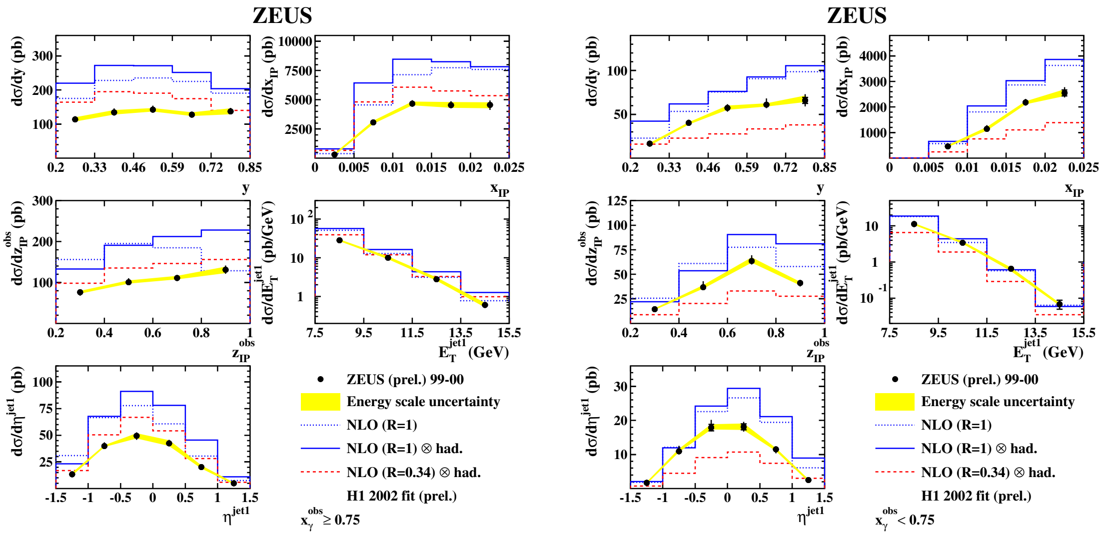

FIGURE 5. Differential cross sections for diffractive dijet photoproduction for a direct-enriched (left) and a resolved-enriched (right) sample. The variable z_{IP} is the longitudinal fractional momentum taken from the diffractive exchange by the dijet system.

bins. For most of these highest x-bins, where there is no previous measurement, the data tend to lie above the expectations from CTEQ6D [4]. Precision measurements at high-x at HERA will allow to constrain the valence parton distributions, where up to now only fixed target experiments at low Q^2 have provided experimental data.

DIFFRACTION

At HERA, NLO QCD fits have also been performed to inclusive diffractive data and diffractive parton distribution functions (dPDFs) have been extracted. Assuming the QCD factorization theorem to be valid, in hard diffractive processes the cross section can be factorized into the partonic cross sections and these dPDFs, which are assumed to be universal. The dPDFs are then used to make predictions for various diffractive final states. Here I will concentrate on diffractive photoproduction of dijets, which were measured in the kinematic range $0.2 < y < 0.85$ and $x_{IP} < 0.025$. Jets were selected with the longitudinally invariant k_T algorithm and with the asymmetric cuts $E_T > 7.5, 6.5$ GeV for the two jets. Double differential cross sections were measured separately in the region $x_\gamma^{obs} < 0.75$, which is the resolved-photon enriched region, and the region $x_\gamma^{obs} > 0.75$, which is the region where direct-photon interactions dominate. The measured distributions in y, x_{IP}, z_{IP} and E_T and η of the highest-E_t jet are shown at the hadron level in figure 5. The data are compared to NLO calculations [5] with diffractive PDFs extracted from the H1 data [6]. In general the NLO calculations (shown by the line $\mathrm{R} = 1$) reproduce the shape of the distributions, but their normalization is too high.

A reduction factor $\mathrm{R} = 0.34$ has been calculated [7] in $p\bar{p}$ diffractive interactions, originating from interactions between spectator partons in the two hadronic beams.

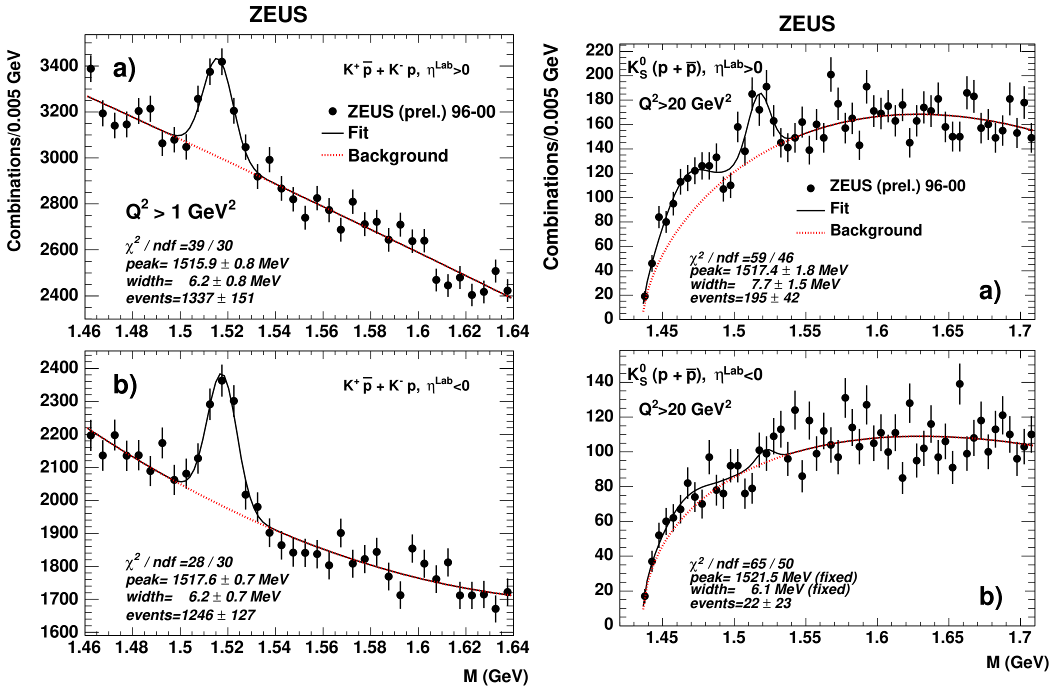

FIGURE 6. Invariant mass spectra for the $\Lambda(1520)$ (left) and for the Θ^+ (right), for $Q^2 > 20$ GeV^2 and divided in forward pseudorapidity region (top) and rear region (bottom). The forward region corresponds to the direction of the proton.

Such rescattering processes create additional particles that fill the large rapidity gap characteristic of diffractive processes, causing a suppression of the measured cross sections and a break of factorization. A similar reduction could be expected for resolved processes in which the photon behaves like a hadron. The dashed curve in figure 5, corresponding to NLO predictions with $\mathrm{R} = 0.34$, is however too low compared to the measured resolved-photon cross sections and a suppression factor of $\mathrm{R} \simeq 0.5$ seems more appropriate. A similar suppression factor seems to be needed also for direct processes, as shown by the left plot of figure 5, although in this case the photon is more point-like and factorization is expected to hold.

EXOTIC FINAL STATES

Recently there has been many experiments reporting evidence of new baryonic states consisting of five quarks. A number of experiments, including ZEUS [8], have observed a narrow resonance decaying either to nK^+ or pK^0_S and with a mass around 1530 MeV, which could correspond to the pentaquark state $\Theta^+ = uudd\bar{s}$. Other experiments have reported negative searches for this state and ZEUS is at the moment the only high energy experiment to have observed the Θ^+ candidate. Recent studies from ZEUS have focused in trying to understand the production mechanism of this state.

The $K^0_S p(\bar{p})$ spectrum was studied for $Q^2 > 20$ GeV^2 separately in the forward proton region, selecting events with $\eta > 0$, and in the rear region, $\eta < 0$. The resulting spectra

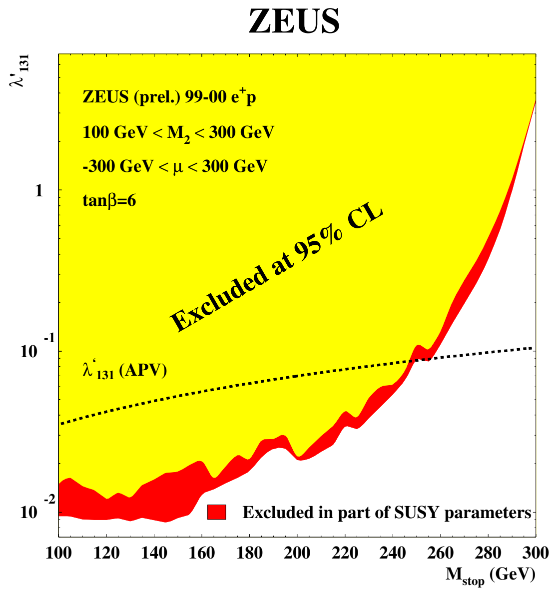

FIGURE 7. Limits on the R-parity-violating coupling λ'_{131} as a function of the stop mass. The light region shows the excluded region for all considered SUSY scenarios, the dark area for a part of them. The dashed line is the limit from atomic-parity violation measurements.

are shown in figure 6: the fitted number of events under the peak is higher in the region closer to the proton remnant, compared to the rear region. This is not what is observed in the production of the $\Lambda(1520) \to K^+p$, as shown in the same figure. This suggests that the production mechanism for the Θ^+ could be different from pure fragmentation in the central rapidity region and could be related to proton-remnant fragmentation.

ZEUS has also performed a search for two other exotic states: the $\theta_C = uudd\bar{c}$ observed by H1 [9] in the HERA I data: and the states $\Xi^{--}_{3/2}$ or $\Xi^{0}_{3/2}$ with a mass around 1860 MeV decaying in $\Xi\pi$, observed by the NA49 Collaboration [10]. The Θ_c was observed by H1 as a narrow resonance at a mass of 3099 GeV decaying to D^*p, both in a $Q^2 > 1$ GeV^2 sample and in a photoproduction sample: approximately 1% of the selected D^* mesons were observed to come from the decay of a Θ_C. A similar analysis was performed by ZEUS [11] in an inclusive sample with approximately 60,000 D^* candidates, but no evidence for this state was found. Also a search [12] for the two states observed by NA49, decaying respectively to $\Xi^-\pi^-$ or $\Xi^-\pi^+$, was performed and no resonance was found in a large mass range nor around the region of 1860 GeV.

R-PARITY-VIOLATING SUSY SEARCHES

HERA is the ideal place to look for possible exotic states originating from the fusion of the initial positron/electron and a valence quark in the proton. Among these, the stop can be produced from $e^+d \to \tilde{t}$ via the R-parity-violating coupling λ'_{131}. The stop can then decay as $\tilde{t} \to e^+d$ or through the decay $\tilde{t} \to b\chi^+$, giving a rich topology of final states. ZEUS has performed a search with the 99-00 e^+p data looking for final state topologies

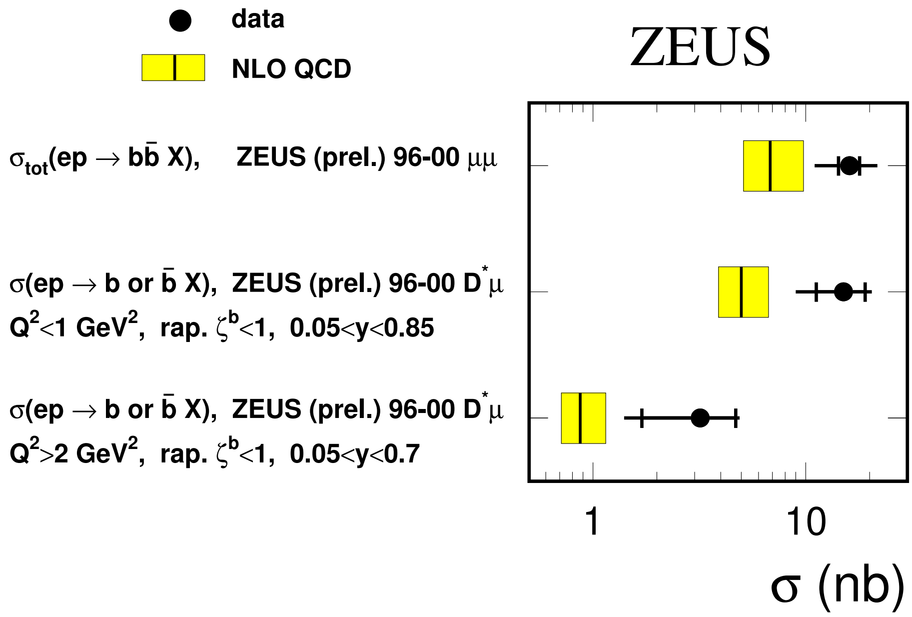

FIGURE 8. Beauty cross section from dimuon and $D^* + \mu$ tagged events. The measurements (dots) are compared to the NLO QCD calculations.

with one positron and one jet (e-J) or multi jets (e-MJ) and one neutrino and multi jets (ν-MJ). The branching ratios to the various channels depend on the SUSY parameters, therefore a scan over a wide range of SUSY parameters was performed. Selection cuts were designed to optimize the signal sensitivity with respect to the main background, which comes from NC and CC interactions at high Q^2. No resonance was observed in the invariant mass of the final state particles in the different topologies, therefore 95% confidence level limits were set on stop production. The results are shown in figure 7 for the stop mass versus the coupling λ'_{131}. The yellow (light) area is the excluded region; the effect of changing the SUSY parameters in a wide range and for $\tan\beta = 6$, as shown in the legend of the figure, is shown by the dark shaded band. The limits for masses up to 250 GeV improve on the low-energy limits from atomic parity violation (APV) measurements and depend weekly on the SUSY parameters.

HEAVY FLAVOURS

Beauty production has been measured by ZEUS both in photoproduction and in DIS. The hard scale provided by the mass of the b-quark allows to compare to NLO QCD calculations. A new measurement based on 121 pb^{-1} of HERA I data in which two muons are observed in the final state was presented at this workshop. Tagging both muons coming from the semileptonic b decays allows a better suppression of the backgrounds from charm and light flavour production. This also means that muons, and therefore b's, can be selected at low p_T and in a large η range, which implies less extrapolation in deriving the total cross section. In addition the normalizations of the various backgrounds can be constrained dividing the sample into high- and low-mass, isolated and non-isolated, like-and unlike-sign muon pairs.

From the visible cross section, a total cross section for beauty production at HERA is extracted and compared to NLO QCD predictions from the sum of the two calculations FMNR (for photoproduction) and HVQDIS (for DIS), obtaining:

$$\sigma^b_{tot}(ep \to b\bar{b}X)[318\ \text{GeV}] = 16.1 \pm 1.8(stat.)^{+5.3}_{-4.8}(syst.)\ \text{nb}, \quad (2)$$

$$\sigma^b_{tot}(\text{NLO}) = 6.9^{+3.0}_{-1.8}\ \text{nb}, \quad (3)$$

where the uncertainties on the theory were evaluated changing the renormalization and factorisation scales by a factor 2 and varying the b mass between 4.5 and 5 GeV.

The result is shown in figure 8, where also previous results from ZEUS, based on $D^* + \mu$ samples [13], are shown. These samples also allow measurement of the cross section to be made for low transverse momentum of the b's. From the figure it looks like there is the tendency for these cross sections to be above NLO QCD predictions, while for higher Q^2 and higher p_T there is good agreement between theory and measurements (see e.g. [14]).

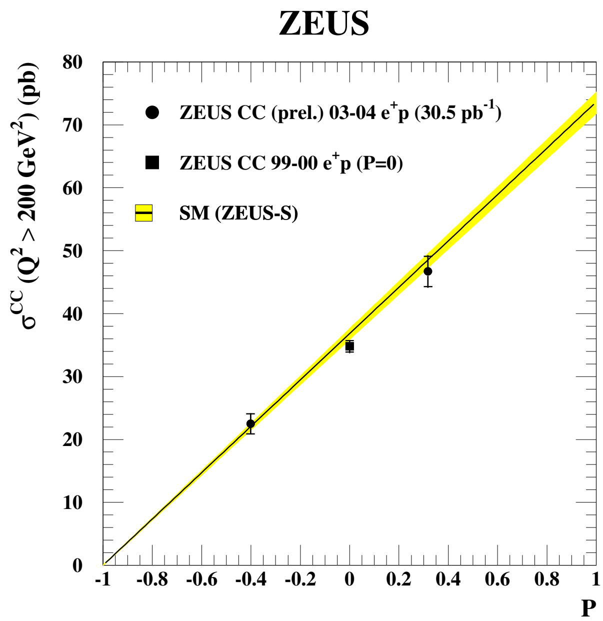

FIGURE 9. Charged current total cross sections as a function of the longitudinal polarization of the positron beam, compared to the SM predictions with the ZEUS-S PDFs. The square symbol shows the HERA I results from the published unpolarized e^+p data.

HERA II

Cross sections at high Q^2

The HERA II running phase has started, e^+p collisions with longitudinally polarized positrons have been collected in 2003-2004 and in 2004-2005 the machine has switched to polarized electron beams. Cross sections at high Q^2 were measured with the first 2003-2004 data with polarized positron beams [15], with a mean luminosity weighted polarization $P = -40.2\%$ for 16.4 pb^{-1} of collected data, and $P = +31.8\%$ for 14.1 pb^{-1} of integrated luminosity. The total charged current cross section is predicted in the Standard Model to have a linear dependence on the polarization, becoming zero for left-handed positrons (or right-handed electrons).

The measured CC cross sections for the two polarization values are shown in figure 9: the linear dependence on P is clearly visible and the points are in good agreement with the SM prediction, which is calculated with the ZEUS-S parton densities for the proton. The effect of the longitudinal polarization in the NC cross sections can only be seen at very high Q^2 with a high integrated luminosity. A marginal effect could anyway already be seen in these data [15].

Charm cross sections

Charm is produced in DIS mainly through the boson-gluon-fusion mechanism and is therefore directly sensitive to the gluon density in the proton. The cross section for charm was measured in 40 pb^{-1} of e^+p and 33 pb^{-1} of e^+p data collected in 2003-2005, as a function of Q^2 in the range $5 < Q^2 < 1000$ GeV^2. Charm was tagged using the $D^* \to D^0\pi_S \to K\pi\pi_S$ decay, where tracks were reconstructed with the central tracking detector and the newly installed silicon microvertex detector. Approximately 1200 D^* candidates were selected in each sample, e^+p and e^-p. The ratio of the cross sections for the two samples was measured, as shown in figure 10, as a function of Q^2. This ratio is particularly interesting as, with the previous published HERA I data [16] (based on 17 pb^{-1} of e^-p and 65 pb^{-1} of e^+p), the D^* production rate was observed to be higher in e^-p than in e^+p, as shown also in the figure. This ratio was found to be 1.67 ± 0.21 (only statistical error) in the range $40 < Q^2 < 1000$ GeV^2 and such phenomenon is not expected from any physics process. With the higher statistics in the e^-p data, collected up to now at HERA II, this effect is not confirmed and the ratio agrees with unity through the whole range of Q^2 measured.

CONCLUSION

The ZEUS Collaboration is completing the analysis of the HERA I data and starting to look at the HERA II data. Recent highlights have been described here; many more results and details can be found in these proceedings from the parallel sessions contributions.

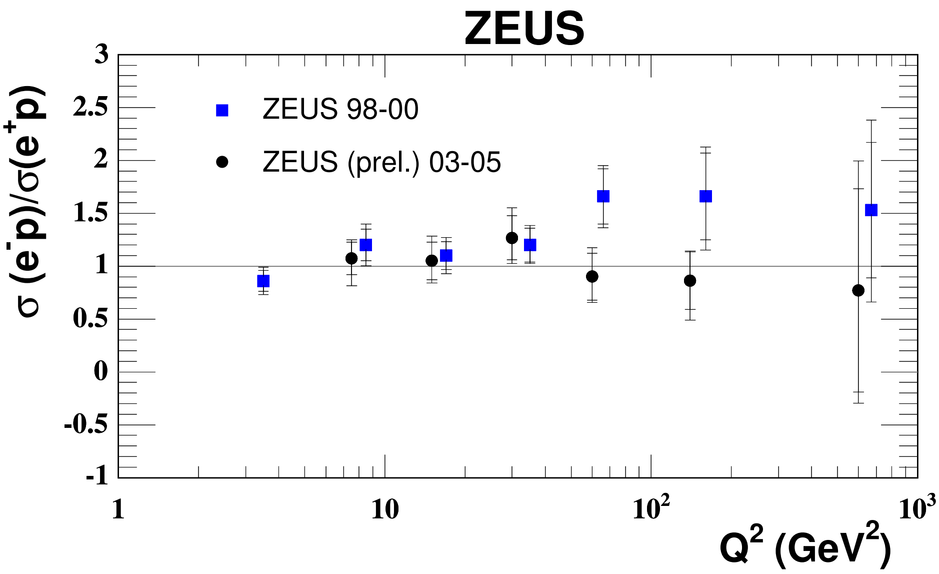

FIGURE 10. The ratio of the cross sections for D^* production in $e^- p$ to the one in $e^+ p$, as measured in the 03-05 data and in the 98-00 data. The inner error bars show the statistical uncertainty, the outer error bar the systematic uncertainty. Many systematic effects cancel in the ratio.

ACKNOWLEDGMENTS

I would like to thank my ZEUS colleagues, and in particular Matthew Wing and Rik Yoshida, for the preparation of this talk; and Prof. Wesley H. Smith for the excellent organization of this Workshop.

REFERENCES

1. ZEUS Collaboration, DESY-05-071 (2005).
2. C. Glasman, these proceedings and references therein (2005).
3. A. H. Mueller, *J. Phys. G*, **19**, 1463–1468 (1993).
4. J. Pumplin et al., *JHEP*, **0207**, 012 (2002).
5. M. Klasen, and G. Kramer, *Eur. Phys. J*, **C38**, 93 (2004).
6. H1 Collaboration, paper 980 submitted to ICHEP02 (2002).
7. A. B. Kaidalov, *Phys. Lett.*, **B567**, 61 (2003).
8. ZEUS Collaboration, *Phys. Lett.*, **B591**, 7–22 (2004).
9. H1 Collaboration, *Phys. Lett.*, **B588**, 17–28 (2004).
10. NA49 Collaboration, *Phys. Rev. Lett.*, **92**, 042003 (2004).
11. ZEUS Collaboration, *Eur. Phys. J.*, **C38**, 29–41 (2004).
12. ZEUS Colaboration, DESY-05-018 (2005).
13. ZEUS Collaboration, paper 5-0342 submitted to ICHEP04 (2004).
14. H1 Collaboration, *Eur. Phys. J.*, **C41**, 453 (2005).
15. ZEUS Collaboration, paper 4-0256 submitted to ICHEP04 (2004).
16. ZEUS Collaboration, *Phys. Rev.*, **D69**, 012004 (2004).